TO APPEAR IN THE ASTROPHYSICAL JOURNAL
Preprint typeset using LaTeX style emulateapj v. 04/03/99

arXiv:astro-ph/0002084v1 3 Feb 2000

X-RAY SPECTRAL AND TIMING EVOLUTION DURING THE DECAY OF THE 1998 OUTBURST FROM THE RECURRENT X-RAY TRANSIENT 4U 1630–47

JOHN A. TOMSICK
Department of Physics and Columbia Astrophysics Laboratory, Columbia Univ., 550 West 120th Street, New York, NY 10027
(Current address: Center for Astrophysics and Space Sciences, Univ. of California, San Diego, MS 0424, La Jolla, CA 92093)
(e-mail: jtomsick@ucsd.edu)
PHILIP KAARET
Harvard-Smithsonian Center for Astrophysics, 60 Garden Street, Cambridge, MA 02138 (e-mail: pkaaret@cfa.harvard.edu)

To Appear in the Astrophysical Journal

ABSTRACT

We report on the X-ray spectral and timing behavior of the recurrent X-ray transient 4U 1630–47 for 51 *RXTE* observations made during the decay of its 1998 outburst. The observations began when the source was still relatively bright, and, during one of the early observations, a QPO with a non-Lorentzian profile occurred near 6 Hz. As the source decayed, the X-ray flux dropped exponentially with an e-folding time of 14.4 d. The exponential decay was interrupted by an increase in the X-ray flux, and a secondary maximum occurred 89 d after the onset of the outburst. A transition marked by significant changes in the timing and spectral properties of the source occurred 104 d after the start of the outburst. The transition is similar to soft-to-hard state transitions observed in other black hole candidate X-ray binaries. Most of the changes associated with the transition occurred in less than 2 d. The timing changes include an increase in the continuum noise level from less than 4% RMS to greater than 10% RMS and the appearance of a quasi-periodic oscillation (QPO) at 3.4 Hz with an RMS amplitude of 7.3% in the 2-21 keV energy band. At the transition, the energy spectrum also changed with an abrupt drop in the soft component flux in the *RXTE* band pass. A change in the power-law photon index from 2.3 to 1.8, also associated with the transition, occurred over a time period of 8 d. After the transition, the source flux continued to decrease, and the QPO frequency decayed gradually from 3.4 Hz to about 0.2 Hz.

Subject headings: accretion, accretion disks — X-ray transients: general — stars: individual (4U 1630–47) — stars: black holes — X-rays: stars

1. INTRODUCTION

Although the recurrent X-ray transient and black hole candidate (BHC) 4U 1630–47 has been studied extensively since its first detected outburst in 1969 (Priedhorsky 1986), interest in this source has intensified due to observations made during its 1998 outburst. During the 1998 outburst, radio emission was detected for the first time (Hjellming et al. 1999). Although the source was not resolved in the radio, the optically thin radio emission suggests the presence of a radio jet. Also, low frequency quasi-periodic oscillations (QPOs) were discovered during the 1998 outburst (Dieters et al. 1998a) using the *Rossi X-ray Timing Explorer* (*RXTE*).

Here, we report on X-ray observations of 4U 1630–47 made with *RXTE* (Bradt, Rothschild & Swank 1993) during the decay of its 1998 outburst. We compare the X-ray light curve to those of other BHC X-ray transients and study the evolution of the spectral and timing properties during the decay. Like many other X-ray transients, the light curve of 4U 1630–47 shows an exponential decay and a secondary maximum (Chen, Shrader & Livio 1997). During the early part of the decay, when the X-ray flux was high, 4U 1630–47 showed canonical soft state characteristics (van der Klis 1995; Nowak 1995; Chen & Taam 1996), including an energy spectrum with a strong soft component and a steep power-law and relatively low timing variability with a fractional RMS (Root-Mean-Square) amplitude of a few percent. Later in the decay, we observe a transition to a spectrally harder and more variable state, which has similarities to transitions observed for GS 1124–68 (Ebisawa et al. 1994; Miyamoto et al. 1994) and GRO J1655–40 (Mendez et al. 1998) near the ends of their outbursts.

In this paper, we describe the 4U 1630–47 X-ray light curve for the 1998 outburst and the *RXTE* observations (§2). In §3 and §4, we present results of modeling the power and energy spectra, respectively. In §5, we examine the transition in more detail, and §6 contains a discussion of the results. Finally, §7 contains a summary of our findings.

2. OBSERVATIONS AND LIGHT CURVE

We analyzed PCA (Proportional Counter Array) and HEXTE (High Energy X-ray Timing Experiment) data from 51 *RXTE* pointings of 4U 1630–47 during the decay of its 1998 outburst. The observation times, integration times and background subtracted 2.5-20 keV PCA count rates are given in Table 1. In Figure 1, we show the 1.5-12 keV PCA fluxes with the ASM (All-Sky Monitor) flux measurements in the same energy band. The ASM light curve was produced from data provided by the ASM/*RXTE* teams at MIT and at the *RXTE* SOF and GOF at NASA's GSFC. The 1998 outburst was first detected by BATSE on Modified Julian Date 50841 (MJD = JD–2400000.5), and 4U 1630–47 was not detected by the ASM until about MJD 50847 (Hjellming et al. 1999; Kuulkers et al. 1998a). Figure 1 shows that the ASM flux increased rapidly after MJD 50850, peaking at 1.10×10^{-8} erg cm^{-2} s^{-1} (1.5-12 keV) on MJD 50867. The flux dropped to about 6×10^{-9} erg cm^{-2} s^{-1} soon after the peak, and our *RXTE* observations began during this time. Our observations fill a gap in the ASM light curve near MJD 50880, showing that a flare occurred during this time.

The flux decayed exponentially between MJD 50883 and MJD 50902 with an e-folding time of 14.4 d. After the exponential decay, the flux increased by about 50% over a time period of about 20 d, and a secondary maximum occurred near MJD 50936. After the secondary maximum, the flux decay is consistent with an exponential with an e-folding time of 12 d to 13 d. In Figure 1, the vertical dashed line at MJD 50951 marks an abrupt change in the timing properties of the source, which is described in detail below. The source flux at the transition was between 6 and 7 $\times 10^{-10}$ erg cm^{-2} s^{-1}.

Soft γ-ray bursts were detected from a position near 4U 1630–47 on MJD 50979 (Kouveliotou et al. 1998), 7 d after our last *RXTE* observation, and the γ-ray source has been named SGR 1627–41. Although the position of SGR 1627–41 is not consistent with the position of 4U 1630–47 (Hurley et al. 1999), the two sources are close enough so that they were both in the *RXTE* field of view during our observations, allowing for the possibility of source confusion. As described in detail in the appendix, *RXTE* scans and *BeppoSAX* observations provide information about possible source confusion. Based on the evidence, we conclude that it is very unlikely that SGR 1627–41 contributed significantly to the flux detected during our observations of 4U 1630–47.

3. X-RAY TIMING

For each observation, we produced 0.0156-128 Hz power spectra to study the timing properties of the system. For each 64 s interval, we made an RMS normalized power spectrum using data in the 2-21 keV energy band. To convert from the Leahy normalization (Leahy et al. 1983) to RMS, we determined the Poisson noise level using the method described in Zhang et al. (1995) with a deadtime of 10 microseconds per event. For each observation, the individual 64 s power spectra were averaged, and the average spectrum was fitted using a least-squares technique and several different analytic models. For individual 64 s power spectra, we calculated the error bars using equation A11 from Leahy et al. (1983). When combining the power spectra for an entire observation, we used two different methods to calculate the errors. In one method, we calculated the errors by propagating the error bars for individual power spectra. This method does not account for any intrinsic (i.e., non-random) changes in the power spectrum over the duration of the observation. We also estimated the error by calculating $\sigma/\sqrt{N}$, where σ is the standard deviation of the power measurements from the individual spectra, and N is the number of 64 s power spectra being combined. For all observations, the error estimates are approximately the same above $\sim$2 Hz, indicating that the shape of the power spectrum at higher frequencies does not change significantly during an observation. However, below $\sim$2 Hz, the calculated errors are significantly larger using the second method, indicating that intrinsic changes in this region of the power spectrum are significant. In the following, we have used the second method to calculate the errors.

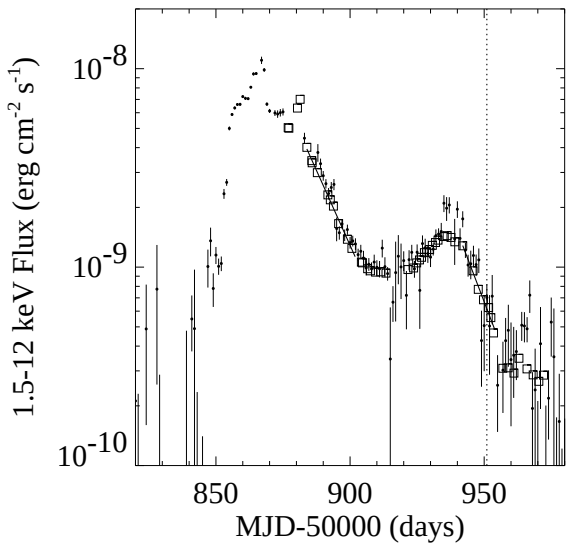

FIG. 1.— X-ray light curve for the 1998 outburst of 4U 1630–47. The points with error bars are 1.5-12 keV ASM daily flux measurements, and the squares mark the 1.5-12 keV fluxes measured by the PCA during 51 pointed observations. The solid lines are exponential fits to the light curve, and the dotted vertical line marks a transition in the spectral and timing properties of the source.

To determine the analytic model to use for the continuum noise, we began by fitting the power spectrum for each observation with a power-law model. For some observations, the power-law fits are acceptable ($\chi^2_\nu \sim 1.0$); however, in most cases, the reduced χ^2 is significantly greater than 1.0 and systematic features appear in the residuals. Strong QPOs dominate the residuals for several observations, and these are discussed in detail below. For the observations without obvious QPOs, the power-law residuals are similar and show a broad excess peaking between 0.5 and 1.0 Hz. To model this broad excess, we focus on the observation 8 power spectrum since the statistics are good for this observation and there are no strong QPOs. Fitting the observation 8 power spectrum with a power-law alone gives a poor fit ($\chi^2/\nu = 680/444$). Previous studies of the power spectra of BHCs show that the continuum noise can be described by a model consisting of two components: A power-law and a band-limited noise component (e.g., Cui et al. 1997; Miyamoto et al. 1994). In applying this model to 4U 1630–47, we used a broken power-law with the lower power-law index fixed to zero for the band-limited component, and hereafter this model is referred to as the flat-top model. Applying this two-component model to the observation 8 power spectrum gives a significantly improved fit ($\chi^2/\nu = 486/441$). Figure 2a shows the observation 8 power spectrum fitted with the two-component model.

For each observation, we fitted the power spectrum using the power-law model alone, the flat-top model alone and the combination of the two components. For several of the observations, the statistics are not good enough to uniquely determine the best continuum model. In these cases, we combined consecutive observations, as indicated in Table 2, to improve the statistics and refitted the power spectra with the same models. For observations 1 to 10, the fit using the two-component model is significantly better than using either of the individual components, indicating that these power spectra require both components. For observations 11 to 51, the flat-top model alone provides a significantly better fit than the power-law model alone, and the two-component model does not provide a significantly better fit

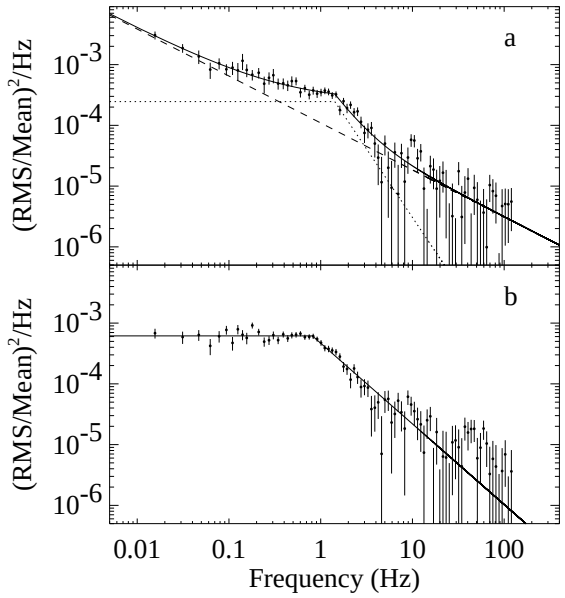

FIG. 2.— The power spectra for observation 8 (a) and observations 11 to 40 (b). The observation 8 power spectrum is fitted with a model consisting of a power-law (dashed line) and a band-limited (or flat-top) noise component (dotted line). The solid line is the sum of the two components. For observations 11 to 40, only the flat-top component (solid line) is necessary. These power spectra have been rebinned for presentation.

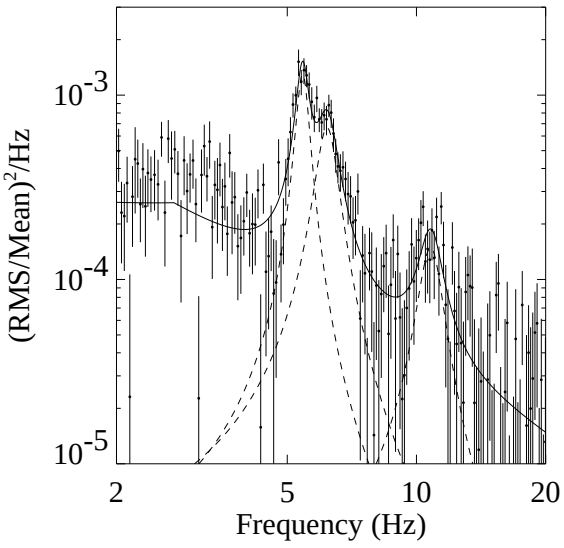

FIG. 3.— Observation 3 power spectrum fitted with the continuum model (flat-top plus power-law) and three Lorentzians at 5.43 Hz, 6.19 Hz and 10.79 Hz (dashed lines). The solid line is the sum of the continuum and the Lorentzians.

than the flat-top component alone. We conclude that only the flat-top component is necessary to fit these power spectra. The continuum parameters for all observations are given in Table 2. In cases where the power-law component is not significantly detected, the 90% confidence upper limit on the contribution from a power-law with an index of -1.0 is given. Figure 2b shows the power spectrum for observations 11 to 40 combined, illustrating that the power-law component is not significant at low frequencies. We note that there is some evidence for excess noise near 45 Hz, but this excess is not statistically significant. For observations 41 to 51, the RMS amplitude for the continuum noise is 10% to 17%, which is considerably higher than for observations 1 to 40. In determining the continuum parameters, we included Lorentzians to model the QPOs as marked in Table 2.

To determine where QPOs are present, we examined the residuals for fits with the continuum model only. For observations 1-2, 3, 6, 7, 8, 41, 42, 43, 44, 45, 46-48 and 49, systematic features in the residuals suggest the presence of QPOs. To determine if these features are statistically significant, we compared the χ^2 for a fit with the continuum model only to a fit with a Lorentzian added to the continuum model. F-tests indicate that QPOs significant at greater than 96% confidence occurred for observations 1-2, 3, 41, 42, 43 and 46-48. For observation 1-2, the continuum model provides a relatively poor fit to the data ($\chi^2/\nu = 561/441$), and the largest residuals occur near 11 Hz. The fit is significantly improved ($\chi^2/\nu = 471/438$) when a Lorentzian is added to the continuum model. The QPO centroid, FWHM and RMS amplitude are 10.8 ± 0.2 Hz, 2.9 ± 0.6 Hz and $2.01\% \pm 0.16\%$, respectively. Although the features for observations 6, 7 and 8 are not as statistically significant, they also have centroids between 10 and 13 Hz and may be related to the observation 1-2 QPO.

For observation 3, the continuum model provides an extremely poor fit ($\chi^2/\nu = 987/441$), and the largest residuals occur near 6 Hz. Although the fit is significantly improved by the addition of a Lorentzian at 5.7 Hz, the fit is still relatively poor ($\chi^2/\nu = 685/438$), and systematic features are present in the residuals, which indicate that the 5.7 Hz QPO is not well-described by a Lorentzian. As for some other BHCs (Belloni et al. 1997; Revnivtsev, Trudolyubov & Borozdin 1999), the QPO has a high frequency shoulder that can be modeled using a second Lorentzian. Modeling the QPO with Lorentzians at 5.4 Hz and 6.2 Hz improves the fit to $\chi^2/\nu = 608/435$. The fit can be further improved to $\chi^2/\nu = 552/432$ by the addition of a QPO near 11 Hz. It is possible that the 11 Hz QPO is a harmonic of the lower frequency QPO, but it may also be related to the QPO that occurred during observation 1-2. Table 3 summarizes the QPO parameters for observation 3, and it should be noted that three Lorentzians were included in the model in determining the continuum parameters given in Table 2. Figure 3 shows the observation 3 power spectrum fitted with a model consisting of the continuum plus three Lorentzians to model the QPOs. The Lorentzians at 5.43 ± 0.02 Hz, 6.19 ± 0.04 Hz and 10.79 ± 0.14 Hz have RMS amplitudes of $2.89\% \pm 0.18\%$, $2.85\% \pm 0.21\%$ and $1.85\% \pm 0.20\%$, respectively. To determine if the QPO properties changed during the observation, we divided observation 3 into two time segments with durations of 576 s and 512 s, made power spectra for each segment and fit-

ted the power spectra with a model consisting of the continuum (flat-top plus power-law) plus three Lorentzians. The results for these fits are given in Table 3. There is no evidence for large changes in the QPO properties between the two time segments.

The increase in the continuum noise level that occurred between observations 40 and 41 was accompanied by the appearance of a QPO at 3.390 ± 0.008 Hz with an RMS amplitude of $7.30\% \pm 0.33\%$. In subsequent observations, the QPO frequency gradually shifted to lower frequency. Figure 4 shows the power spectra for observations 41, 42, 43 and 46-48. After the 3.4 Hz QPO appeared for observation 41, QPOs occurred at 2.613 ± 0.012 Hz, 1.351 ± 0.012 Hz and 0.228 ± 0.003 Hz for observations 42, 43 and 46-48, respectively. We note that the observation 43 QPO shows some evidence for a high frequency shoulder. QPOs with lower statistical significance occurred for observations 44, 45 and 49 with frequencies of 0.430 ± 0.006 Hz, 0.365 ± 0.011 Hz and 0.182 ± 0.005 Hz. It should be noted that these QPOs are consistent with the gradual shift to lower frequencies. The QPO parameters for observations 41 to 49 are given in Table 4.

4. ENERGY SPECTRA

We produced PCA and HEXTE energy spectra for each observation using the processing methods described in Tomsick et al. (1999). We used the PCA in the 2.5-20 keV energy band and HEXTE in the 20-200 keV energy band. For the PCA, we used standard mode data, consisting of 129-bin spectra with 16 s time resolution, included only the photons from the top anode layers and estimated the background using the sky-VLE model[1]. We used the version 2.2.1 response matrices with a resolution parameter of 0.8 and added 1% systematic errors to account for uncertainties in the PCA response. As described in Tomsick et al. (1999), we used Crab spectra to test the response matrices and found that the response matrix calibration is better for PCUs 1 and 4 than for the other three Proportional Counter Units (PCUs); thus, we only used these two PCUs for spectral analysis and allowed for free normalizations between PCUs. PCU 4 was off during three observations (34, 39 and 48), and, to avoid instrumental differences, we did not use these observations in our spectral analysis. Previously, we found that the PCA over-estimates the source flux by a factor of 1.18 (Tomsick et al. 1999), and, in this paper, we reduced the fluxes and spectral component normalizations by a factor of 1.18 so that the PCA flux scale is in agreement with previous instruments.

HEXTE energy spectra were produced using standard mode data, consisting of 64-bin spectra with 16 s time resolution. We used the March 20, 1997 HEXTE response matrices and applied the necessary deadtime correction (Rothschild et al. 1998). For the spectral fits, the normalizations were left free between cluster A and cluster B. It is well-known that the HEXTE and PCA normalizations do not agree, so the normalizations were left free between HEXTE and the PCA. The HEXTE background subtraction is performed by rocking on and off source. Each cluster has two background fields, and we checked the HEXTE background subtraction by comparing the count rates for the two fields. In cases where contamination of one of the fields occurred, we only used the data from the non-contaminated background field.

We first fitted the energy spectra using a power-law with interstellar absorption, but this model does not provide acceptable fits to any of the spectra. For most of the observations, the residuals suggest the presence of a soft component, which is typical for 4U 1630–47 (Tomsick, Lapshov & Kaaret 1998; Parmar et al. 1997). A soft component was also detected during *BeppoSAX* observations of 4U 1630–47, which overlap with our *RXTE* observations (Oosterbroek et al. 1998). Since Oosterbroek et al. (1998) found that a disk-blackbody model (Makishima et al. 1986) provides a good description of the soft component observed by *BeppoSAX*, we added a disk-blackbody model to the power-law component and refitted the *RXTE* spectra. Although the addition of a soft component improves the fits significantly in most cases, the fits are only formally acceptable for a small fraction of the observations, and, in the worst case, the reduced χ^2 is 3.1 for 106 degrees of freedom.

A broad iron absorption edge, associated with the Compton reflection component (Lightman & White 1988), is commonly observed in the energy spectra of BHCs (Ebisawa et al. 1994 and references therein; Sobczak et al. 1999). We refitted the 4U 1630–47 spectra with the model given in equation 3 of Ebisawa et al. (1994), which includes a broad absorption edge in addition to the disk-blackbody and power-law components.

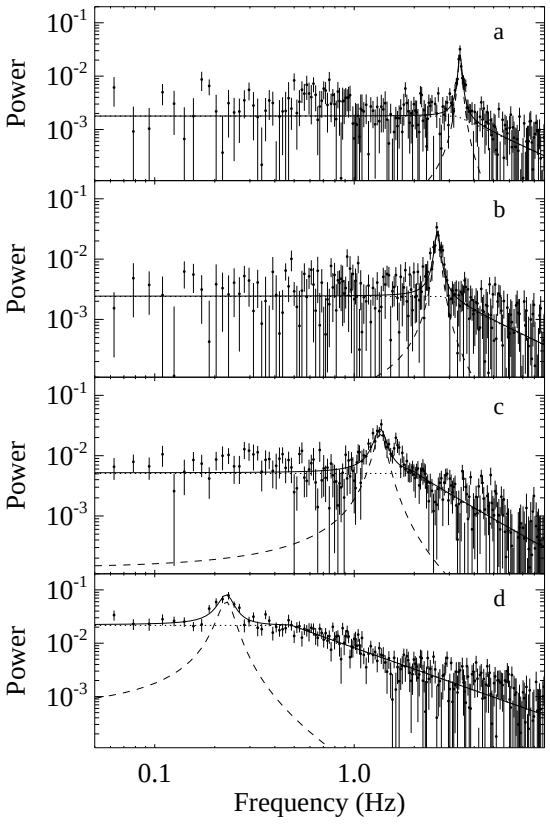

FIG. 4.— Power spectra (Power = (RMS/Mean)^2/Hz) for observations 41 (a), 42 (b), 43 (c) and 46-48 (d) showing QPOs detected at 3.390 Hz, 2.613 Hz, 1.351 Hz and 0.228 Hz. The power spectra are fitted with a model consisting of a flat-top (dotted line) and a Lorentzian (dashed line). The solid line is the sum of the two components.

[1]See M.J. Stark et al. 1999, PCABACKEST, available at http://lheawww.gsfc.nasa.gov/docs/xray/xte/pca.

Following Ebisawa et al. (1994), we fixed the width of the absorption edge to 10 keV and left the edge energy free. For all of the 4U 1630–47 observations, the fits are significantly better with the absorption edge. As an example, for observation 8, the fit improved from $\chi^2/\nu = 179/106$ using the disk-blackbody plus power-law model without the edge to $\chi^2/\nu = 110/104$, indicating that the edge is required at the 99.1% confidence level. In addition to the absorption edge, an iron emission line is expected due to fluorescence of the X-ray illuminated accretion disk material (Matt et al. 1992); thus, we have added an emission line to our model to determine whether the line is present in the spectra. We used a narrow emission line since the width of the emission line could not be constrained, and the energy of the emission line was a free parameter.

We fitted the spectra with the column density free and also with the column density fixed to the mean value for the 51 observations, 9.45×10^{22} cm^{-2}. For all observations, the quality of the fit is not significantly worse with the column density fixed. Table 5 shows the results for the spectral fits with the column density fixed using a model consisting of a power-law, a disk-blackbody component, a narrow emission line and a broad absorption edge. The free parameters for the power-law component are the photon index (Γ) and the normalization. For the disk-blackbody component, the temperature at the inner edge of the disk (kT_{in}) and the normalization are free parameters. Rather than the power-law and disk-blackbody normalizations, the component fluxes are given in Table 5. The emission line energy (E_{line}) and normalization (N_{line}) and the edge energy (E_{edge}) and optical depth ($\tau_{\rm Fe}$) are free parameters. However, in cases where the best fit value for E_{edge} is less than 7.1 keV (the value for neutral iron), we fixed E_{edge} to 7.1 keV. In Table 5, we do not give error estimates for kT_{in} since the uncertainty for this parameter is dominated by systematic error due to uncertainty in the correct value for the column density. By comparing the values found for kT_{in} with the column density fixed to those with the column density free, we estimate that the systematic error is 0.05 keV. For the 51 observations, the largest χ^2_ν is 1.32 for 102 degrees of freedom and $\chi^2_\nu < 1.0$ for 44 of the observations, indicating that the spectra are well-described by the model. Figure 5 shows the observation 8 energy spectrum and residuals. The residuals shown in Figure 5 typify the quality obtained for the observations.

For each observation, we determined the significance of the emission line by refitting the spectra without the line and using an F-test. In cases where the significance of the emission line is less than 90%, we fixed E_{line} to the best fit value and determined the 90% confidence upper limit on N_{line}. Although most of the spectra do not require the emission line at a high confidence level, the line is required at greater than 90% confidence for 16 of the 51 observations, and at greater than 95% confidence for 9 observations. In the cases where the iron line is detected at greater than 90% confidence, the equivalent width of the iron line is between 45 eV (for observation 7) and 110 eV (for observation 47).

We also determined the significance of the disk-blackbody component using the same method described above for the emission line. With the column density fixed, the disk-blackbody component is required at greater than 97% confidence for every observation; however, with the column density free, the disk-blackbody component is not required for several observations. With the column density free, the disk-blackbody components are significant at only 50% and 65% confidence for observations 3 and 4, respectively, and at between 46% and 70% confi-

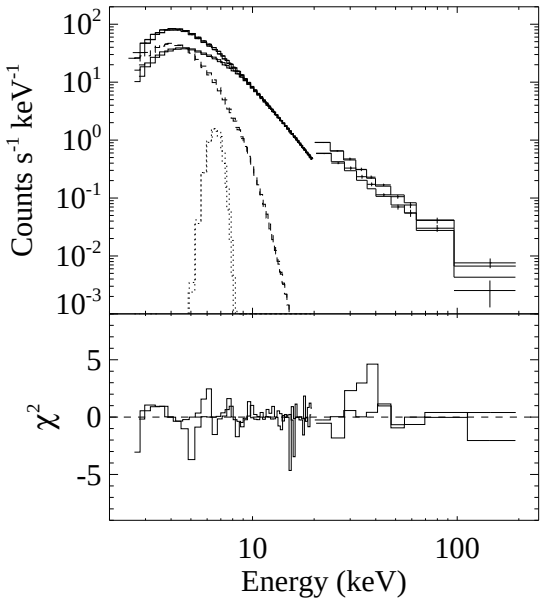

FIG. 5.— PCA and HEXTE energy spectrum for observation 8 folded with the instrument response and fitted with a model consisting of a disk-blackbody (dashed line), a power-law (thin solid line), a narrow emission line (dotted line) and a broad iron absorption edge. The sum of these components is marked with a thick solid line. The column density is fixed to 9.45×10^{22} cm^{-2}. The bottom panel shows the residuals for the fit.

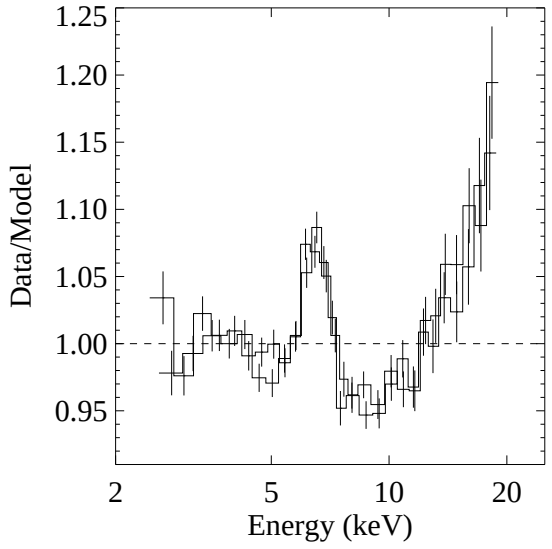

FIG. 6.— Data-to-model ratio for a power-law plus disk-blackbody fit to the spectrum for observations 44 to 51. An emission line at 6.46 ± 0.04 keV with an equivalent width of 91 eV is clearly present. Although we fitted both the PCA and the HEXTE data, only the PCA data are shown.

dence for observations 41 to 51. In Table 5, the disk-blackbody fluxes for these observations are marked as upper limits since the component is not detected. For observations 41 to 51, the best fit values of kT_{in} are also marked as upper limits since the peak of the disk-blackbody flux falls below the PCA band pass and we cannot constrain kT_{in} and the column density independently.

The flux levels and line parameters are similar for observations 44 to 51 so we refitted the combined spectrum for these observations. As shown in Table 5, an emission line at 6.46 ± 0.04 keV is detected at 99.93% confidence. The line energy is consistent with emission from neutral or mildly ionized iron and the line equivalent width is 91 eV. We also fitted the combined spectrum with a model consisting of a disk-blackbody and a power-law, and Figure 6 shows the data-to-model ratio, clearly indicating the presence of the iron line. Since 4U 1630–47 lies along the Galactic ridge (l = 336.91°, b = 0.25°), we have considered the possibility that the 4U 1630–47 spectra are contaminated by Galactic ridge emission. It is unlikely that the ridge emission is the source of the iron line detected in our spectra because the line energy we observe is considerably lower than the values measured by *ASCA*, *Ginga* and *Tenma* for the Galactic ridge, which are all near 6.7 keV (Kaneda et al. 1997 and references therein). Also, based on the spectrum of the Galactic ridge emission measured by *RXTE* (Valina & Marshall 1998), the spatially averaged Galactic ridge 2.5-20 keV flux is only 6% of the flux for the combination of observations 44 to 51, indicating that the level of contamination by the Galactic ridge emission should be low.

5. STATE TRANSITION

Figure 7 shows the evolution of the timing and spectral parameters for observations 33 to 51. Significant changes in the 4U 1630–47 emission properties occurred between observations 40 and 41, and we interpret this as evidence that a state transition occurred. In Figure 7, the transition is marked with a vertical dashed line at MJD 50951. At the transition, an increase in source variability occurred with the 0.01-10 Hz RMS amplitude of the flat-top component increasing from between 2.1% and 3.9% for observations 33 to 40 to $10.2\% \pm 0.6\%$ for observation 41. As shown in panel b_1 of Figure 7, the RMS amplitude continued to increase after the transition, reaching a maximum value of $17.3\% \pm 0.8\%$ for observation 46-48. In addition to the increase in the continuum noise level, a QPO appeared for observation 41, and the centroid QPO frequency and RMS amplitude are shown in panels b_2 and b_3, respectively. The timing changes occurred in less than 2 d and with only a small change in the 1.5-12 keV flux (shown in panel a of Figure 7).

To determine if a QPO was present before the transition, we made a combined power spectrum for observations 33 to 40. When the 2-21 keV power spectrum is fitted with a flat-top model, the residuals show no clear evidence for a QPO. The 90% confidence upper limit on the RMS amplitude for a QPO in a frequency range from 0.1 Hz to 10 Hz is 2.4%. We performed an additional test by determining the energy range where the observation 41 QPO is strongest. For observation 41, the RMS amplitudes are $6.1\% \pm 0.4\%$ and $8.6\% \pm 0.4\%$ for the 2-6 keV and 6-21 keV energy bands, respectively, indicating

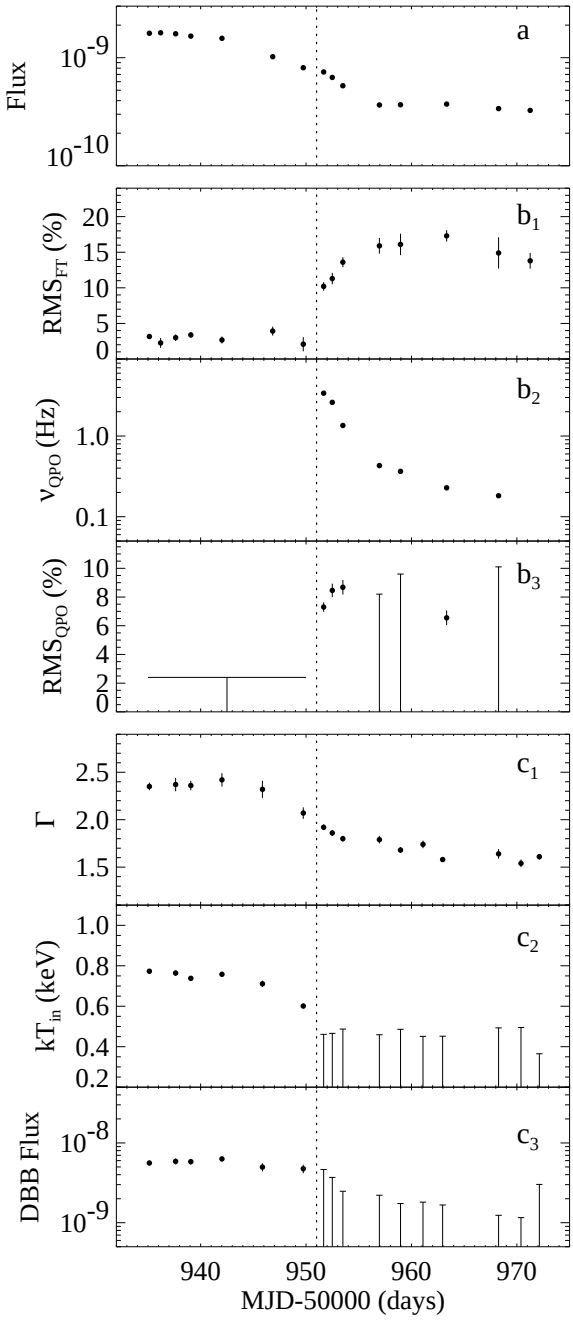

FIG. 7.— Timing and Spectral parameters for observations 33 to 51. Panel a is the 2.5-20 keV flux (in ergs cm^{-2} s^{-1}) vs. time. The timing parameters are shown in panels b_1, b_2 and b_3, and the spectral parameters are shown in panels c_1, c_2 and c_3. The error bars displayed correspond to $\Delta\chi^2 = 1.0$ (68% confidence) and the upper limits shown are 90% confidence. The bolometric disk-blackbody flux is shown in panel c_3. A vertical dotted line at MJD 50951 marks the state transition.

that the strength of the QPO increases with energy. Since the QPO is stronger in the 6-21 keV energy band for observation 41, we produced a 6-21 keV power spectrum for observations 33 to 40. As before, when a flat-top model is used to fit the power spectrum, the residuals do not show evidence for QPOs, and the 90% confidence upper limit on the RMS amplitude for a QPO in a frequency range from 0.1 Hz to 10 Hz is 2.9%.

Although the difference between the observation 40 and 41 energy spectra is not as distinct as for the power spectra, changes occurred. In Figure 7, the spectral parameters Γ and kT_{in} are shown in panels c_1 and c_2, respectively. The power-law index hardened slightly between observations 40 and 41; however, this change appears to be part of a larger trend, which occurred over a span of 8 d between observations 38 and 43. The inner disk temperature began to decrease near observation 37, and the soft component is not confidently detected after observation 40, which probably indicates that kT_{in} continued to drop after observation 40. The spectral changes are also illustrated in Figures 8a and 8b, which show the energy spectra for observations 40 and 41, respectively. Figure 8c shows the energy spectrum for observations 44 to 51, indicating that the spectrum continued to harden after the transition.

In summary, during the transition, the noise level increased, the power-law spectral index hardened and the soft component flux in the *RXTE* band pass decreased. Similar changes are typically observed in BHC systems when soft-to-hard state transitions occur (van der Klis 1995; Nowak 1995; Chen & Taam 1996), and we conclude that such a transition occurred for 4U 1630–47. We also show that QPOs were not present during the observations leading up to the transition, indicating that their appearance during observation 41 is related to the state transition.

6. DISCUSSION

6.1. *Comparisons to Previous 4U 1630–47 Outbursts*

Since 4U 1630–47 was discovered in 1969, quasi-periodic outbursts have been observed from this source every 600 to 690 d (Kuulkers et al. 1997)[2]. The light curve for the 1998 4U 1630–47 outburst is the best example of a "fast-rise exponential-decay" (or FRED) light curve (Chen et al. 1997) that has been observed for 4U 1630–47. A FRED light curve may have been observed for 4U 1630–47 by the *Vela* 5*B* X-ray monitor in 1974 (Priedhorsky 1986; Chen et al. 1997), but the temporal coverage was sparse compared to the coverage obtained for the 1998 outburst. Good temporal coverage was obtained for the 1996 outburst by the *RXTE*/ASM, and a FRED light curve was not observed. After the start of the 1996 outburst, the flux stayed at a high level for about 100 d before decaying exponentially with an e-folding time of about 14.9 d (Kuulkers et al. 1997). Although the overall light curve shapes are different for the two outbursts, it is interesting that the e-folding time for the 1998 outburst, 14.4 d, is close to the 14.9 d e-folding time for the 1996 outburst. This may suggest that the e-folding time is related to a physical property of the system that does not change between outbursts. For example, the e-folding time may be related to the mass of the compact object (Cannizzo, Chen & Livio 1995) or the radius of the accretion disk (King & Ritter 1998).

[2]However, the 1999 outburst significantly deviates from this periodicity (McCollough et al. 1999).

A state transition with similarities to the soft-to-hard transition we report in this paper was observed by *EXOSAT* during the decay of the 1984 outburst from 4U 1630–47. Four *EXOSAT* observations of 4U 1630–47 were made during outburst decay (Parmar, Stella & White 1986). During the first two observations in 1984 April and 1984 May, a strong soft component was observed in the energy spectrum. The power-law was harder in May than in April and became even harder for two observations made in 1984 July. During the July observations, the soft component was not clearly detected. Assuming a soft-to-hard transition occurred between May and July, the transition took place at a luminosity between 10^{36} erg s^{-1} and 10^{38} erg s^{-1} (1-50 keV), which is consistent with the luminosity where the 1998 soft-to-hard transition occurred, 7×10^{36} erg s^{-1} (2.5-20 keV). The luminosities given here are for an assumed

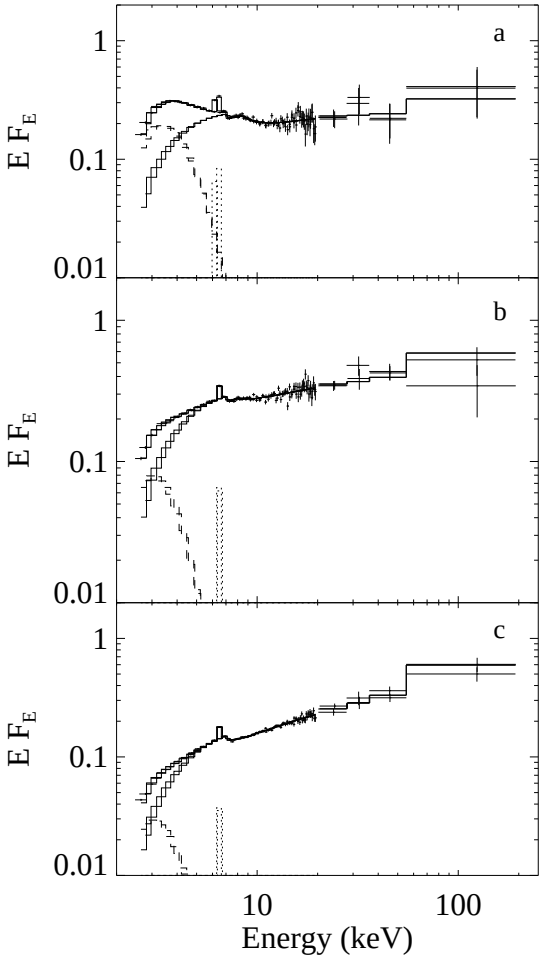

FIG. 8.— Unfolded PCA and HEXTE energy spectra for (a) Observation 40; (b) Observation 41; and (c) Observations 44 to 51 with the spectral components marked as for Figure 5. The figure shows that the disk-blackbody temperature changes significantly between observations 40 and 41, and that the disk-blackbody flux is significantly lower for observations 44 to 51. Also, the power-law gradually hardens.

distance of 10 kpc; however, the distance to 4U 1630–47 is not well-determined.

6.2. *Comparisons to Other Black Hole Candidate X-Ray Transients*

Here, we compare the properties 4U 1630–47 displayed during the decay of its 1998 outburst to those observed for other X-ray transients. We have compiled a list of comparison sources using Tanaka & Shibazaki (1996) and Chen, Shrader & Livio (1997). The comparison group contains the BHC X-ray transients that had strong soft components during outburst and FRED light curves. The comparison sources from the above references are GS 1124–68, GS 2000+251, A 0620–00, EXO 1846–031, Cen X-2, 4U 1543–47 and A 1524–617. We also include a recent X-ray transient, XTE J1748–288, that has similar properties to this group. For the eight comparison sources, the exponentially decaying portions of their X-ray light curves have e-folding times ranging from 15 d to 80 d (Chen et al. 1997; Revnivtsev et al. 1999), and the mean decay time is 39 d. Thus, the 14.4 d e-folding time for 4U 1630–47 is shorter than average, but not unprecedented.

Like 4U 1630–47, secondary maxima occurred in the X-ray light curves of 4U 1543-47, A 0620–00, GS 2000+251 and GS 1124–68, and a tertiary maximum occurred for A 0620–00 (Kaluzienski et al. 1977). It is likely that the secondary and tertiary maxima are the result of X-ray irradiation of the outer accretion disk or the optical companion (King & Ritter 1998; Chen, Livio & Gehrels 1993; Augusteijn, Kuulkers & Shaham 1993). In this picture, the time between the start of the outburst and subsequent maxima depends on the viscous time scale of the disk. For A 0620–00, GS 2000+251 and GS 1124–68, secondary maxima are observed 55 to 75 d after the start of the outburst. These maxima, often referred to as "glitches", consist of a sudden upward shift in X-ray flux, interrupting the exponential decay. The tertiary maximum observed for A 0620–00 about 200 d after the start of the outburst is significantly different, and can be described as a broad (35 to 40 d) bump in the X-ray light curve near the end of the outburst. The 4U 1630–47 secondary maximum is similar to the A 0620–00 tertiary maximum since it is a broad (about 25 d) increase in flux near the end of the outburst. However, the secondary maximum peaked about 89 d after the start of the outburst, which is considerably less than for A 0620–00.

Four sources in our comparison group exhibited soft-to-hard state transitions during outburst decay: A 0620–00 (Kuulkers et al. 1998b), GS 2000+251 (Tanaka & Shibazaki 1996), GS 1124–68 (Kitamoto et al. 1992) and XTE J1748–288 (Revnivtsev et al. 1999). The 4U 1630–47 transition occurred 104 d after the start of the outburst, while transitions for the other four sources occurred 100 to 150 d, 230 to 240 d, 131 to 157 d and about 40 d after the starts of the outbursts for A 0620–00, GS 2000+251, GS 1124–68 and XTE J1748–288, respectively. Detailed X-ray spectral and timing information is available after the transition to the hard state for GS 1124–68. Like 4U 1630–47, the GS 1124–68 transition was marked by an increase in the RMS noise amplitude; however, in contrast to 4U 1630–47, QPOs were not observed for GS 1124–68 in the hard state (Miyamoto et al. 1994). Also, during the GS 1124–68 transition, the X-ray spectrum hardened with a drop in the inner disk temperature (kT_{in}) and a change in the power-law photon index (Γ) from 2.2 to 1.6 (Ebisawa et al. 1994). During the 4U 1630–47 transition, the change in the soft component was consistent with a drop in kT_{in}, and Γ changed from 2.3 to 1.8. While the *Ginga* observations of GS 1124–68 were relatively sparse near the transition, our observations of 4U 1630–47 show that soft-to-hard transitions can occur on a time scale of days.

6.3. *Hard State QPOs*

Although QPOs were not detected after the GS 1124–68 state transition, QPOs were observed after a similar transition for the microquasar GRO J1655–40 during outburst decay (Mendez et al. 1998). *RXTE* observations of GRO J1655–40 show that a state transition occurred between 1997 August 3 and 1997 August 14. The transition was marked by an increase in the continuum variability from less than 2% RMS to 15.6% RMS, a decrease in the characteristic temperature of the soft spectral component (kT_{in}) from 0.79 keV to 0.46 keV and the appearance of a QPO at 6.46 Hz with an RMS amplitude of 9.8%. A QPO was also detected at 0.77 Hz during an August 18 *RXTE* observation of GRO J1655–40 when the 2-10 keV flux was about a factor of four lower than on August 14; thus, the shift to lower frequencies with decreasing flux is common to GRO J1655–40 and 4U 1630–47. The correlations between spectral and timing properties for the microquasar GRS 1915+105 are similar to those observed for GRO J1655–40 and 4U 1630–47. Markwardt, Swank & Taam (1999) and Muno, Morgan & Remillard (1999) found that 1-15 Hz QPOs are observed for GRS 1915+105 more often when the source spectrum is hard. Markwardt et al. (1999) report a correlation between QPO frequency and disk flux, and Muno et al. (1999) find that the QPO frequency is correlated with kT_{in}. Although these results suggest that the QPO is related to the soft component, the fact that the QPO strength increases with energy for 4U 1630–47, GRO J1655–40 and GRS 1915+105 indicates that the QPO mechanism modulates the hard component flux.

A physical model that has been used to explain the energy spectra of BHC systems involves the presence of an advection-dominated accretion flow or ADAF (Narayan, Garcia & McClintock 1997). The model assumes the accretion flow consists of two zones: An optically thin ADAF region between the black hole event horizon and a transition radius, r_t, and a geometrically thin, optically thick accretion disk outside r_t. Esin, McClintock & Narayan (1997) developed and used this model to explain the spectral changes observed for GS 1124–68 during outburst decay, which are similar to the spectral changes observed for 4U 1630–47. The different emission states observed during the decay can be reproduced by decreasing the mass accretion rate and increasing r_t. This model suggests that the gradual decrease in the QPO frequencies observed for GRO J1655–40 and 4U 1630–47 may be related to a gradual increase in r_t or a gradual drop in the mass accretion rate (or both).

In studies of the X-ray power spectra of BHC and neutron star X-ray binaries, Wijnands & van der Klis (1999) find a correlation between the frequency of QPOs between 0.2 and 67 Hz and the break frequency of the continuum component

(described as a flat-top component in this paper). Such a correlation is interesting since it suggests that there is a physical property of the system that sets both time scales and that the physical property does not depend on the different properties of BHCs and neutron stars. While 4U 1630–47 was in its hard state, the break frequency gradually decreased from 3.33 ± 0.36 Hz to 0.48 ± 0.03 Hz between observations 41 and 46-48 as the QPO frequency dropped from 3.4 Hz to 0.23 Hz (cf. see Tables 2 and 4). As for the other sources included in the Wijnands & van der Klis (1999) sample, 4U 1630–47 exhibits a correlation between QPO frequency and break frequency. However, for 4U 1630–47, the QPO frequency is below or consistent with the break frequency, while in other sources the QPO frequency is above the break frequency.

6.4. *Emission Properties During the Flare*

Figure 9 shows the 2-60 keV PCA light curves for the two observations made during the flare which occurred around MJD 50880 (observations 3 and 4). For observation 3, short (about 4 s) X-ray dips are observed. We have examined the light curves for all 51 observations and find that X-ray dips are only observed for observation 3. However, 4U 1630–47 observations made by another group show that short X-ray dips were observed earlier in the outburst (Dieters et al. 1999). In addition to the dips, Figure 9 shows that the level of variability is much higher for observation 3 than for observation 4. Table 2 details the differences between the power spectra for these two observations. For observation 3, the flat-top and power-law RMS amplitudes are 3.55% and 4.36%, respectively, while, for observation 4, the flat-top and power-law RMS amplitudes are 1.83% and 1.10%, which are even lower than most of the nearby non-flare observations. Also, QPOs are observed for observation 3 but not for observation 4. The timing differences between these two observations are especially remarkable because the energy spectra for observations 3 and 4 are nearly identical (cf. Table 5).

The asymmetry of the low frequency QPO peak for observation 3 is similar to QPOs observed for GS 1124–68 (Belloni et al. 1997) and XTE J1748–288 (Revnivtsev et al. 1999). For these two sources and for 4U 1630–47, the asymmetric shape of the QPO can be modeled using two Lorentzians, suggesting that the asymmetry may be due to a shift in the QPO centroid during the observation. Revnivtsev et al. (1999) find that some properties of the XTE J1748–288 power spectra are consistent with this picture. The 4U 1630–47 timing properties during observation 3 are not consistent with a gradual shift in the QPO centroid during the observation since the 5.4 Hz and 6.2 Hz Lorentzians are present in both segments of the observation (cf. Table 3). The stability of the QPO shape may indicate that the asymmetric peak is caused by an intrinsic property of the QPO mechanism. However, for observations of 4U 1630–47 containing dips, Dieters et al. (1999) find that the frequencies of some QPOs are lower within the dips than outside the dips. For our observation 3, it is possible that frequency changes during the dips (cf. Figure 9) cause the QPO profile to be asymmetric.

7. SUMMARY AND CONCLUSIONS

We have analyzed data from 51 *RXTE* observations of 4U 1630–47 during the decay of its 1998 outburst to study the evolution of its spectral and timing properties. During the decay, the X-ray flux dropped exponentially with an e-folding time of about 14.4 d, which is short compared to most other BHC X-ray transients. The e-folding time was nearly the same (14.9 d) for the decay of the 1996 outburst, which may indicate that this time scale is set by some property of the system that does not change between outbursts. For the 1998 outburst, the decay was interrupted by a secondary maximum, which is commonly observed for BHC X-ray transients.

Our analysis of the 4U 1630–47 power spectra indicates that 0.2 Hz to 11 Hz QPOs with RMS amplitudes between 2% and 9% occurred during the observations. During one of our early observations, when the source was relatively bright, a QPO occurred near 6 Hz with a profile that cannot be described by a single Lorentzian. Similar asymmetric QPO peaks have been observed previously for GS 1124–68 (Belloni et al. 1997) and XTE J1748–288 (Revnivtsev et al. 1999). For all three sources (4U 1630–47, GS 1124–68 and XTE J1748–288), the QPO is well-described by a combination of two Lorentzians.

Near the end of the outburst, an abrupt change in the 4U 1630–47 spectral and timing properties occurred, and we interpret this change as evidence for a soft-to-hard state transition. Our observations indicate that most of the changes in the emission properties, associated with the transition, occurred over a time period less than 2 d. The timing properties changed after the transition with an increase in the continuum noise level and the appearance of a QPO. A 3.4 Hz QPO appeared immediately after the transition, and, in subsequent observations, the QPO frequency decreased gradually to about 0.2 Hz. At the transition,

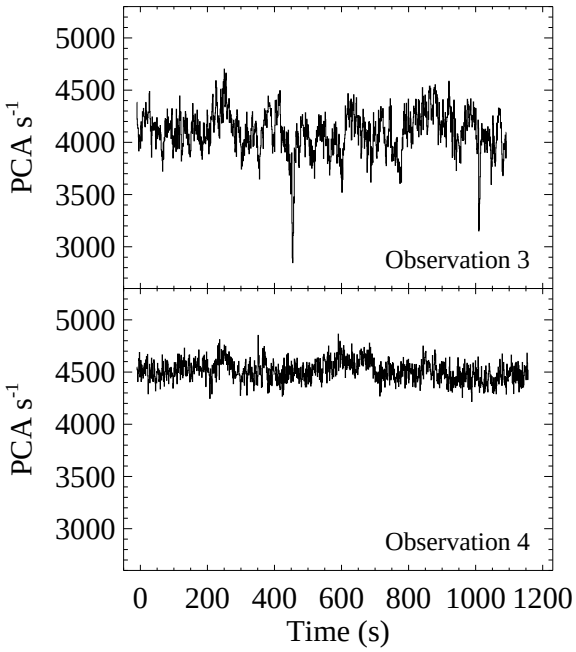

FIG. 9.— PCA light curves for the flare observations (observations 3 and 4). The 2-21 keV X-rays are binned in 1 s intervals, and background has not been subtracted. The figure shows that the source variability was much higher during observation 3 than during observation 4.

the energy spectrum also changed with an abrupt drop in the soft component flux in the *RXTE* band pass, which was probably due to a drop in the inner disk temperature. A change in the power-law photon index from 2.3 to 1.8, also associated with the transition, occurred over a time period of 8 d. Although many of these changes are typical of soft-to-hard state transitions, the QPO behavior and the short time scale for the transition are not part of the canonical picture for state transitions (van der Klis 1995; Nowak 1995; Chen & Taam 1996). Finally, we note that 4U 1630–47 exhibits interesting behavior (e.g., state changes and QPOs) below a flux level of 10^{-9} erg cm^{-2} s^{-1}, indicating that observing programs for X-ray transients should be designed to follow these sources to low flux levels.

The authors would like to thank J.H. Swank for approving observations of 4U 1630–47 at low flux levels, S. Dieters for providing results from *BeppoSAX* observations prior to publication and an anonymous referee whose comments led to an improved paper. We acknowledge partial support from NASA grants NAG5-4633, NAG5-4416 and NAG5-7347.

REFERENCES

Augusteijn, T., Kuulkers, E. & Shaham, J. 1993, A&A 279, L13
Belloni, T. et al. 1997, A&A 322, 857
Bradt, H.V., Rothschild, R.E. & Swank, J.H. 1993 A&AS 97, 355
Cannizzo, J.K., Chen, W. & Livio, M. 1995, ApJ 454, 880
Chen, W., Livio, M. & Gehrels, N. 1993, ApJ 408, L5
Chen, W., Shrader, C.R. & Livio, M. 1997, ApJ 491, 312
Chen, X. & Taam, R.E. 1996, ApJ 466, 404
Cui, W. et al. 1997, ApJ 484, 383
Dieters, S. et al. 1998a, IAUC 6823
Dieters, S. et al. 1998b, IAUC 6962
Dieters, S. et al. 1999, astro-ph/9912028
Ebisawa, K. et al. 1994, PASJ 46, 375
Esin, A.A., McClintock, J.E. & Narayan, R. 1997, ApJ 489, 865
Hjellming, R.M. et al. 1999, ApJ 514, 383
Hurley, K. et al. 1998a, IAUC 6948
Hurley, K. et al. 1998b, IAUC 6966
Hurley, K. et al. 1999, ApJ 519, L143
Kaluzienski, L.J., Holt, S.S., Boldt, E.A. & Serlemitsos, P.J. 1977, ApJ 212, 203
Kaneda, H. et al. 1997, ApJ 491, 638
King, A.R. & Ritter, H. 1998, MNRAS 298, L42
Kitamoto, S. et al. 1992, ApJ 394, 609
Kouveliotou, C. et al. 1998, IAUC 6944
Kuulkers, E., Parmar, A.N., Kitomoto, S., Cominsky, L.R., Sood, R.K. 1997, MNRAS 291, 81
Kuulkers, E. et al. 1998a, IAUC 6822
Kuulkers, E. 1998b, astro-ph/9805031
Leahy, D.A. et al. 1983, ApJ 266, 160
Lightman, A.P. & White, T.R. 1988, ApJ 335, 57
Makishima, K. et al. 1986, ApJ 308, 635
Markwardt, C.B., Swank, J.H. & Taam, R.E. 1999, ApJ 513, L37
Matt, G. et al. 1992, A&A 257, 63
McCollough, M.L., Harmon, B.A., Dieters, S., Wijnands, R. 1999, IAUC 7165
Mendez, M. et al. 1998, ApJ 499, L187
Miyamoto, S. et al. 1994, ApJ 435, 398
Muno, M.P., Morgan, E.H. & Remillard, R.A. 1999, astro-ph/9904087
Narayan, R., Garcia, M.R. & McClintock, J.E. 1997, ApJ 478, L79
Nowak, M.A. 1995, PASP 107, 1207
Oosterbroek, T. et al. 1998, A&A 340, 431
Parmar, A.N., Stella, L. & White, N.E. 1986, ApJ 304, 664
Parmar et al. 1997, A&A 319, 855
Priedhorsky, W.C. 1986, Ap&SS 126, 89
Revnivtsev, M.G., Trudolyubov, S.P. & Borozdin, K.N. 1999, astro-ph/9903306
Rothschild et al. 1998, ApJ 496, 538
Sobczak et al. 1999, ApJ 520, 776
Tanaka, Y. & Shibazaki, N. 1996, ARA&A 34, 607
Tomsick, J.A., Kaaret, P., Kroeger, R.A. & Remillard, R.A. 1999, ApJ 512, 892
Tomsick, J.A., Lapshov, I. & Kaaret, P. 1998, ApJ 494, 747
Valina, A. & Marshall F.E. 1998, ApJ 505, 134
Van der Klis, M. 1995, in X-Ray Binaries, W.H.G. Lewin, J. van Paradijs & E.P.J. van den Heuvel (Eds.), Cambridge University Press, p. 252
Wijnands, R. & van der Klis, M. 1999, ApJ 514, 939
Woods, P.M. et al. 1999, ApJ 519, L139
Zhang, W. et al. 1995, ApJ 449, 930

APPENDIX

SGR 1627–41

Soft γ-ray bursts were detected from a position near 4U 1630–47 on MJD 50979 (Kouveliotou et al. 1998), 7 d after our last *RXTE* observation. The soft γ-ray repeater, SGR 1627–41, was observed with *RXTE* on MJD 50990, and a 0.15 Hz QPO was detected during the observation (Dieters et al. 1998b). Although the position of SGR 1627–41 is not consistent with the position of 4U 1630–47 (Hurley et al. 1999), the two sources are close enough so that they were both in the *RXTE* field of view during the observation made on MJD 50990 and also during our observations, allowing for the possibility of source confusion. We inspected the *RXTE* 0.125 s light curves for our 4U 1630–47 observations, and there is no evidence for activity (e.g., bursts) from SGR 1627–41. An *RXTE* scanning observation made on 1998 June 21 (MJD 50985) and *BeppoSAX* observations made on 1998 August 7 (MJD 51032) and 1998 September 16 (MJD 51072) provide information about possible source confusion. The scanning observation indicates that 4U 1630–47 was much brighter than SGR 1627–41 on June 21. Below, we present an analysis of the data from the scanning observation. 4U 1630–47 was also much brighter than SGR 1627–41 during the *BeppoSAX* observations. On August 7 and September 16, the 2-10 keV unabsorbed flux for 4U 1630–47 was 30 to 40 times higher than for SGR 1627–41 (Woods et al. 1999; Dieters et al. 1999). It is likely that 4U 1630–47 also dominated the flux detected during the June 26 *RXTE* observation and that it is responsible for the 0.15 Hz QPO. Given the low persistent flux detected for SGR 1627–41 by *BeppoSAX*, 6.7×10^{-12} erg cm^{-2} s^{-1} unabsorbed in the 2-10 keV band (Woods et al. 1999), it seems very unlikely that this source could be bright enough to produce the QPOs observed during our observations.

After soft γ-ray bursts were detected from SGR 1627–41 by BATSE (Burst and Transient Source Experiment) on 1998 June 15 (Kouveliotou et al. 1998), *RXTE* scanning observations were made to locate a source of persistent X-ray emission related to soft γ-ray repeater (SGR). When the scans were made, the position of SGR 1627–41 was restricted to the IPN (3rd Interplanetary Network) annulus reported in Hurley et al. (1998a), which is consistent with the position of the supernova remnant G337.0-0.1. *RXTE* scans were made along the IPN annulus on 1998 June 19 and nearly perpendicular to the IPN annulus on 1998 June 21. Since other SGRs are associated with supernova remnants, the perpendicular scan was centered on G337.0-0.1. In the following months, the IPN position was improved (Hurley et al. 1998b) and a source of persistent X-ray emission related to the SGR was discovered using *BeppoSAX* (Woods et al. 1999). These observations restrict the SGR 1627–41 position to a $2'$ by $16''$ region that is consistent with the position of G337.0-0.1, making an association between the two likely (Hurley et al. 1999).

TABLE 1
RXTE OBSERVATIONS OF 4U 1630–47

Observation	MJD[a]	Integration Time (s)	PCA count rate[b] (s^{-1})
1	50876.9325	1824	3158
2	50877.1978	1712	3135
3	50880.3884	1136	4005
4	50881.3865	1232	4420
5	50883.9011	7248	2453
6	50885.7305	2832	2108
7	50885.8687	6432	2051
8	50887.8010	9920	1826
9	50891.7337	9152	1400
10	50892.6314	4816	1313
11	50893.8026	9456	1212
12	50895.7370	9424	992
13	50899.0084	1200	822
14	50900.6819	912	736
15	50904.2146	992	626
16	50904.6203	9328	621
17	50906.5668	7056	587
18	50907.5942	9920	568
19	50909.5107	11120	553
20	50911.3969	9920	559
21	50913.3997	11040	547
22	50921.5827	576	599
23	50923.6826	9824	587
24	50924.8245	10128	634
25	50925.8665	1584	653
26	50926.6551	400	692
27	50927.7248	512	714
28	50928.5927	416	723
29	50929.6599	560	741
30	50930.6609	608	772
31	50931.8622	544	801
32	50932.7974	800	825
33	50935.1336	1136	854
34	50936.1995	1024	873
35	50937.6251	512	847
36	50939.0651	736	799
37	50942.0190	672	758
38	50945.8624	352	571
39	50947.8040	960	467
40	50949.7373	864	404
41	50951.6677	1328	397
42	50952.4870	880	361
43	50953.4910	1408	307
44	50956.9571	1440	201
45	50958.9578	1312	208
46	50961.0918	912	194
47	50962.9571	1440	240
48	50965.9570	1616	207
49	50968.2637	624	193
50	50970.3910	720	145
51	50972.1303	864	203

[a]Modified Julian Date (MJD = JD–2400000.5) at the midpoint of the observation.

[b]2.5-20 keV count rate for 5 PCUs (all 3 layers) after background subtraction.

TABLE 2
POWER SPECTRA: CONTINUUM PARAMETERS[a]

	Flat-top			Power-law		
Obs.	RMS[b](%)	ν_{break} (Hz)	α	RMS[b](%)	α	χ^2/ν
1-2[e]	3.24 ± 0.21	0.49 ± 0.05	-0.96 ± 0.04	1.37 ± 0.66	-1.56 ± 0.19	471/438
3[e]	3.55 ± 0.21	2.72 ± 0.28	-1.46 ± 0.15	4.36 ± 0.72	-1.70 ± 0.07	552/432
4	1.83 ± 0.33	1.52 ± 0.66	-0.73 ± 0.11	1.10 ± 0.56	-1.52 ± 0.24	495/441
5	2.04 ± 0.28	2.54 ± 0.50	-1.23 ± 0.28	1.98 ± 0.32	-0.97 ± 0.08	418/441
6[e]	2.71 ± 0.27	1.42 ± 0.14	-1.90 ± 0.33	1.60 ± 0.48	-1.05 ± 0.16	453/438
7[e]	2.49 ± 0.18	1.72 ± 0.10	-2.87 ± 0.54	2.47 ± 0.23	-0.89 ± 0.05	405/438
8[e]	2.48 ± 0.18	1.40 ± 0.09	-2.24 ± 0.38	2.38 ± 0.15	-0.81 ± 0.04	470/438
9-10	2.67 ± 0.22	1.60 ± 0.14	-1.69 ± 0.24	2.06 ± 0.25	-0.75 ± 0.07	431/441
11-12	3.52 ± 0.16	0.56 ± 0.04	-1.05 ± 0.04	< 1.0[c]	-1.0[d]	518/443
13-24	3.65 ± 0.12	0.76 ± 0.04	-1.33 ± 0.06	< 0.7[c]	-1.0[d]	421/443
25-40	3.13 ± 0.27	1.57 ± 0.14	-2.82 ± 0.71	< 1.0[c]	-1.0[d]	452/443
41[e]	10.2 ± 0.6	3.33 ± 0.36	-1.73 ± 0.24	< 2.5[c]	-1.0[d]	480/440
42[e]	11.3 ± 0.8	2.81 ± 0.33	-1.60 ± 0.21	< 3.6[c]	-1.0[d]	415/440
43[e]	13.6 ± 0.7	1.97 ± 0.12	-1.87 ± 0.16	< 3.3[c]	-1.0[d]	479/440
44[e]	15.9 ± 1.1	0.83 ± 0.07	-1.45 ± 0.10	< 5.2[c]	-1.0[d]	550/440
45[e]	16.1 ± 1.5	0.55 ± 0.06	-1.31 ± 0.08	< 2.0[c]	-1.0[d]	491/440
46-48[e]	17.3 ± 0.8	0.48 ± 0.03	-1.33 ± 0.05	< 5.4[c]	-1.0[d]	453/440
49[e]	14.9 ± 2.2	0.26 ± 0.05	-1.45 ± 0.12	< 9.0[c]	-1.0[d]	550/440
50-51	13.8 ± 1.1	0.19 ± 0.02	-1.28 ± 0.08	< 8.3[c]	-1.0[d]	494/440

[a]The errors correspond to $\Delta\chi^2 = 1.0$ (68% confidence).

[b]0.01-10 Hz RMS amplitudes.

[c]90% confidence upper limit.

[d]Power-law index fixed to this value.

[e]A Lorentzian is included in the model. For observation 3, three Lorentzians are included in the model as described in the text.

TABLE 3
QPO PARAMETERS FOR OBSERVATION 3[a]

	All of Observation 3			Time Segment 1[b]	Time Segment 2[c]
	1 Lorentzian	2 Lorentzians	3 Lorentzians	3 Lorentzians	3 Lorentzians
ν_1 (Hz)	5.74 ± 0.03	5.42 ± 0.02	5.43 ± 0.02	5.49 ± 0.02	5.35 ± 0.03
$FWHM_1$ (Hz)	1.06 ± 0.07	0.37 ± 0.06	0.41 ± 0.06	0.38 ± 0.05	0.49 ± 0.10
RMS_1 (%)	4.03 ± 0.10	2.76 ± 0.19	2.89 ± 0.18	2.95 ± 0.20	2.88 ± 0.25
ν_2 (Hz)	—	6.17 ± 0.05	6.19 ± 0.04	6.17 ± 0.06	6.25 ± 0.06
$FWHM_2$ (Hz)	—	0.77 ± 0.13	0.78 ± 0.12	0.71 ± 0.16	0.85 ± 0.17
RMS_2 (%)	—	2.85 ± 0.22	2.85 ± 0.21	2.60 ± 0.25	3.09 ± 0.27
ν_3 (Hz)	—	—	10.79 ± 0.14	11.00 ± 0.19	10.57 ± 0.18
$FWHM_3$ (Hz)	—	—	1.47 ± 0.45	2.00 ± 0.63	1.56 ± 0.53
RMS_3 (%)	—	—	1.85 ± 0.20	2.11 ± 0.24	1.95 ± 0.26
χ^2/ν	685/438	608/435	552/432	570/432	480/432

[a]The errors correspond to $\Delta\chi^2 = 1.0$ (68% confidence).

[b]First 576 seconds of Observation 3.

[c]Last 512 seconds of Observation 3.

TABLE 4
QPO PARAMETERS FOR OBSERVATIONS 41-49[a]

Observation	Frequency (Hz)	FWHM (Hz)	RMS (%)
41	3.390 ± 0.008	0.14 ± 0.02	7.30 ± 0.33
42	2.613 ± 0.012	0.17 ± 0.03	8.46 ± 0.47
43	1.351 ± 0.012	0.22 ± 0.04	8.68 ± 0.51
44	0.430 ± 0.006	0.07 ± 0.02	< 8.2[b]
45	0.365 ± 0.011	0.11 ± 0.04	< 9.6[b]
46-48	0.228 ± 0.003	0.046 ± 0.010	6.55 ± 0.51
49	0.182 ± 0.005	0.043 ± 0.012	< 10.1[b]

[a]The errors correspond to $\Delta\chi^2$ = 1.0 (68% confidence).

[b]90% confidence upper limit.

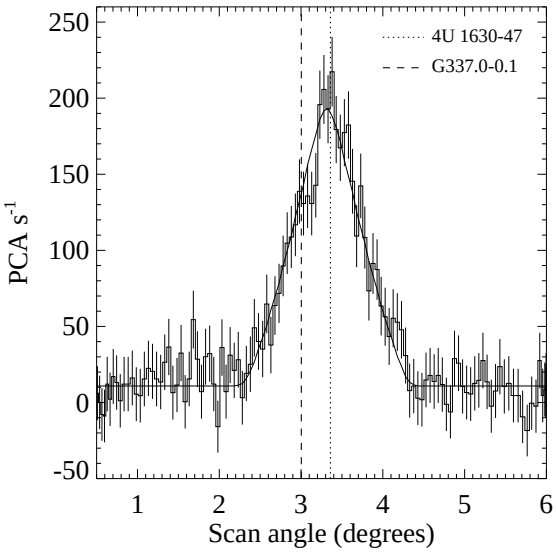

FIG. A1.— The PCA light curve for the scan performed on June 21, showing that X-ray emission was coming from a position consistent with the 4U 1630–47 position (dotted line). It is likely that SGR 1627–41 is associated with the supernova remnant G337.0-0.1 (Hurley et al. 1999) and its position is also marked (dashed line).

We analyzed the *RXTE* data from the June 21 scan to determine if the persistent X-ray emission from SGR 1627–41 could have been bright enough to contaminate our *RXTE* observations of 4U 1630–47. The linear scan passed through the positions of both G337.0-0.1 and 4U 1630–47 for this purpose. Figure A1 shows the background subtracted 2-60 keV PCA count rate versus scan angle. We fitted the light curve using a model consisting of a single point source and a constant count rate offset to account for small uncertainties in the background subtraction. We used the 1996 June 5 PCA collimator response to model the scan light curve produced by a point source. A good fit is achieved (χ^2/ν = 91/161), indicating that the light curve is consistent with the presence of one source. Figure A1 shows that the source position is consistent with 4U 1630–47 and not G337.0-0.1. Also, the source amplitude is about 187 s^{-1} (2-60 keV, 5 PCUs), which is close to the count rates reported for observations 44 to 51 in Table 1. The *RXTE* scan indicates that it is very unlikely that our 4U 1630–47 observations are significantly contaminated by emission from SGR 1627–41.

TABLE 5
ENERGY SPECTRUM FIT PARAMETERS[a,b]

	Power-law		Disk-blackbody		Narrow Emission Line			Broad Absorption Edge		
Obs.	Γ	F_{PL}[c]	kT_{in} (keV)	F_{DBB}[d]	E_{line} (keV)	N_{line}[e]	Signif. (%)	E_{edge}	$\tau_{\rm Fe}$	χ^2/ν
1	2.498 ± 0.019	7.42	0.955	7.95	6.60[g]	< 2.6[f]	72.8	8.65 ± 0.16	0.84 ± 0.09	80/102
2	2.389 ± 0.017	7.34	0.917	8.66	6.68[g]	< 3.1[f]	78.8	9.05 ± 0.13	0.94 ± 0.08	135/102
3	2.603 ± 0.015	10.6	1.577	< 2.79	6.41[g]	< 2.4[f]	52.3	8.71 ± 0.34	0.43 ± 0.10	96/102
4	2.557 ± 0.012	10.3	1.573	< 5.08	6.79[g]	< 1.9[f]	67.0	9.15 ± 0.32	0.35 ± 0.08	107/102
5	2.500 ± 0.021	3.70	1.049	11.5	6.63[g]	< 2.3[f]	87.3	9.00 ± 0.09	1.50 ± 0.10	90/102
6	2.402 ± 0.023	3.99	0.933	9.62	6.70 ± 0.07	1.9 ± 0.5	94.7	8.93 ± 0.10	1.42 ± 0.10	104/102
7	2.457 ± 0.016	4.09	0.905	9.14	6.61 ± 0.08	1.7 ± 0.5	93.2	8.77 ± 0.09	1.36 ± 0.08	92/102
8	2.453 ± 0.016	3.50	0.914	8.61	6.63 ± 0.07	1.6 ± 0.4	97.4	8.76 ± 0.08	1.47 ± 0.08	78/102
9	2.412 ± 0.017	2.61	0.861	7.94	6.60 ± 0.07	1.2 ± 0.3	93.6	8.55 ± 0.08	1.55 ± 0.08	90/102
10	2.396 ± 0.023	2.38	0.857	7.96	6.65 ± 0.07	1.2 ± 0.3	94.4	8.61 ± 0.09	1.78 ± 0.10	93/102
11	2.444 ± 0.020	2.14	0.847	7.83	6.52 ± 0.06	1.3 ± 0.3	97.4	8.59 ± 0.07	1.84 ± 0.09	104/102
12	2.276 ± 0.015	2.14	0.714	7.13	6.43 ± 0.07	1.0 ± 0.3	97.7	8.37 ± 0.08	1.46 ± 0.07	78/102
13	2.265 ± 0.040	1.67	0.733	6.28	6.49[g]	< 1.5[f]	88.2	8.57 ± 0.15	1.56 ± 0.17	97/102
14	2.265 ± 0.042	1.63	0.666	6.30	6.25[g]	< 1.3[f]	78.6	8.22 ± 0.18	1.43 ± 0.19	83/102
15	2.264 ± 0.050	1.37	0.664	5.45	6.32[g]	< 1.2[f]	85.1	8.37 ± 0.18	1.49 ± 0.22	87/102
16	2.248 ± 0.017	1.43	0.636	5.58	6.47[g]	< 0.8[f]	88.8	8.08 ± 0.10	1.40 ± 0.09	64/102
17	2.122 ± 0.017	1.41	0.605	5.22	6.49 ± 0.07	0.6 ± 0.2	92.9	8.23 ± 0.11	1.24 ± 0.09	77/102
18	2.136 ± 0.016	1.39	0.595	5.09	6.49 ± 0.06	0.7 ± 0.2	96.3	8.44 ± 0.09	1.30 ± 0.08	86/102
19	2.074 ± 0.015	1.28	0.643	4.95	6.50 ± 0.05	0.7 ± 0.2	96.5	8.31 ± 0.09	1.49 ± 0.08	100/102
20	2.264 ± 0.021	1.14	0.701	4.81	6.54 ± 0.06	0.7 ± 0.2	98.2	8.31 ± 0.09	1.61 ± 0.10	73/102
21	2.330 ± 0.024	1.05	0.718	4.93	6.50 ± 0.06	0.7 ± 0.2	98.7	8.45 ± 0.09	1.75 ± 0.10	87/102
22	2.064 ± 0.050	1.40	0.633	4.97	6.38[g]	< 1.0[f]	63.0	8.20 ± 0.24	1.34 ± 0.24	101/102
23	2.202 ± 0.021	1.24	0.701	4.20	6.56 ± 0.05	0.8 ± 0.2	99.5	8.61 ± 0.08	1.75 ± 0.09	90/102
24	2.185 ± 0.017	1.43	0.681	4.68	6.49[g]	< 0.8[f]	87.3	8.13 ± 0.10	1.35 ± 0.09	90/102
25	2.180 ± 0.036	1.45	0.693	4.83	6.59[g]	< 1.1[f]	82.6	8.32 ± 0.18	1.30 ± 0.16	88/102
26	2.158 ± 0.066	1.46	0.723	4.69	6.31[g]	< 1.6[f]	73.5	8.18 ± 0.33	1.22 ± 0.29	84/102
27	2.269 ± 0.065	1.51	0.731	5.10	6.48[g]	< 1.2[f]	60.4	8.14 ± 0.27	1.42 ± 0.28	94/102
28	2.466 ± 0.068	1.64	0.706	4.74	6.32[g]	< 1.1[f]	54.5	7.95 ± 0.42	0.99 ± 0.29	93/102
29	2.320 ± 0.071	1.52	0.760	4.89	6.77[g]	< 1.4[f]	66.4	8.71 ± 0.28	1.27 ± 0.28	92/102
30	2.364 ± 0.064	1.58	0.762	5.25	6.56[g]	< 1.4[f]	72.0	8.46 ± 0.19	1.68 ± 0.25	104/102
31	2.370 ± 0.060	1.70	0.757	5.08	6.33[g]	< 1.3[f]	65.3	8.31 ± 0.26	1.29 ± 0.25	88/102
32	2.268 ± 0.048	1.73	0.750	5.40	6.35 ± 0.08	1.3 ± 0.4	90.1	8.53 ± 0.19	1.44 ± 0.20	73/102
33	2.348 ± 0.042	1.73	0.773	5.68	6.55[g]	< 1.3[f]	70.7	8.09 ± 0.18	1.52 ± 0.19	81/102
35	2.367 ± 0.067	1.70	0.764	5.99	6.62[g]	< 1.0[f]	53.2	8.24 ± 0.18	2.10 ± 0.28	111/102
36	2.356 ± 0.052	1.67	0.738	5.75	6.39[g]	< 1.2[f]	63.2	8.40 ± 0.18	1.62 ± 0.22	89/102
37	2.422 ± 0.068	1.40	0.758	6.24	6.36[g]	< 1.3[f]	73.3	8.37 ± 0.19	1.89 ± 0.19	85/102
38	2.317 ± 0.092	1.12	0.711	5.01	6.65[g]	< 0.8[f]	51.0	8.38 ± 0.39	1.28 ± 0.39	81/102
40	2.072 ± 0.058	0.90	0.601	4.78	6.33 ± 0.07	0.8 ± 0.3	99.96	8.47 ± 0.18	1.73 ± 0.27	75/102
41	1.916 ± 0.027	1.09	< 0.461	< 4.69	6.45[g]	< 0.8[f]	80.1	8.06 ± 0.22	0.92 ± 0.18	107/102
42	1.858 ± 0.032	1.00	< 0.466	< 3.57	6.43[g]	< 0.6[f]	58.4	7.74 ± 0.25	1.08 ± 0.22	63/102
43	1.798 ± 0.027	0.85	< 0.487	< 2.42	6.51[g]	< 0.6[f]	71.8	7.49 ± 0.27	0.91 ± 0.19	98/102
44	1.793 ± 0.037	0.56	< 0.459	< 2.19	6.44[g]	< 0.4[f]	61.6	7.54 ± 0.29	1.05 ± 0.26	74/102
45	1.675 ± 0.031	0.58	< 0.486	< 1.68	6.46[g]	< 0.6[f]	85.6	7.1[g]	1.36 ± 0.27	89/103
46	1.735 ± 0.038	0.55	< 0.451	< 1.83	6.54[g]	< 0.6[f]	73.4	7.1[g]	1.19 ± 0.33	78/103
47	1.584 ± 0.024	0.67	< 0.452	< 1.70	6.47 ± 0.07	0.5 ± 0.2	93.0	7.1[g]	0.66 ± 0.22	74/103
49	1.640 ± 0.055	0.54	< 0.493	< 1.27	6.34[g]	< 0.7[f]	68.3	7.56 ± 0.32	1.45 ± 0.37	83/102
50	1.536 ± 0.040	0.50	< 0.495	< 1.21	6.50[g]	< 0.7[f]	74.5	7.1[g]	0.98 ± 0.36	99/103
51	1.605 ± 0.031	0.57	< 0.365	< 3.20	6.40[g]	< 0.6[f]	72.7	7.1[g]	0.78 ± 0.28	94/103
44-51	1.657 ± 0.012	0.58	< 0.455	< 1.83	6.46 ± 0.04	0.4 ± 0.1	99.93	7.1[g]	1.08 ± 0.11	98/103

[a]Column density fixed to 9.45×10^{22} cm^{-2}.

[b]The errors correspond to $\Delta\chi^2 = 1.0$ (68% confidence).

[c]2.5-20 keV unabsorbed flux in units of 10^{-9} erg cm^{-2} s^{-1}.

[d]Bolometric flux in units of 10^{-9} erg cm^{-2} s^{-1}.

[e]Normalization in units of 10^{-3} photons cm^{-2} s^{-1}.

[f]90% confidence upper limit.

[g]Fixed.